JACS
JOURNAL OF THE AMERICAN CHEMICAL SOCIETY
Communication
pubs.acs.org/JACS

Unexpected Catalytic Performance in Silent Tantalum Oxide through Nitridation and Defect Chemistry

Yiguo Su,[†] Junyu Lang,[†] Liping Li,[‡] Kai Guan,[†] Chunfang Du,[†] Liman Peng,[†] Dan Han,[†] and Xiaojing Wang*,[†]

[†]College of Chemistry and Chemical Engineering, Inner Mongolia University, Hohhot 010021, P. R. China

[‡]Key Lab of Optoelectronic Materials Chemistry and Physics, Fujian Institute of Research on the Structure of Matter, Chinese Academy of Sciences, Fuzhou 350002, P. R. China

Supporting Information

ABSTRACT: This work reports on the preparation of a noble-metal-free and highly active catalyst that proved to be an efficient and green reductant with renewable capacity. Nitridation of a silent $Ta_{1.1}O_{1.05}$ substrate led to the formation of a series of TaO_xN_y hollow nanocrystals that exhibited outstanding activity toward catalytic reduction of nitrobenzenes under ambient conditions. ESR and XPS results indicated that defective nitrogen species and oxygen vacancies at the surfaces of the TaO_xN_y nanocrystals may play synergetic roles in the reduction of nitrobenzenes. The underlying mechanism is completely different from those previously reported for metallic nanoparticles. This work may provide new possibilities for the development of novel defect-meditated catalytic systems and offer a strategy for tuning any catalysts from silent to highly reactive by carefully tailoring the chemical composition and surface defect chemistry.

Oxidation/reduction reactions at nanoparticle (NP) surfaces play key roles in remission of the environmental and energy crises and in other processes such as catalytic production of highly valuable chemicals, geochemical redox formation, and dissolution of minerals.[1] In particular, the reduction of substituted nitrobenzenes to the corresponding anilines is of great importance because anilines are among the most important organic intermediates necessary for the manufacture of many valuable products such as dyestuffs, pharmaceuticals, and agricultural chemicals.[2] The key to conversion of nitrobenzenes to the corresponding anilines is the selection of a suitable reducing agent, which determines the reaction conditions, efficiency, and/or selectivity of the conversion reaction. One effective approach in the laboratory is to use the commercially available reductant $NaBH_4$ with catalysis by free or immobilized NPs in aqueous solution at ambient temperature. A significant number of investigations have been devoted to creating new multifunctional NPs for the efficient reduction of nitrobenzenes.[3] However, the majority of investigations have focused merely on metallic NPs, especially noble-metal NPs. From the viewpoint of unprecedented practical applications, it is highly necessary to explore noble-metal-free and highly active catalysts and comprehend the underlying chemistry and physics.

It is widely accepted that the chemical activity of NPs is closely related to the number and nature of surface defects, which are governed by the structure, chemical composition, morphology, and size of the NPs.[4] Since oxygen vacancies, surface cations, and surface hydrogen species are silent in the reduction of nitrobenzenes,[5] tuning the NP surface for unique defect structures seems to be urgently essential. Nitridation is highly promising in this regard because the crystal structure, electronic structure, and surface properties of NPs are usually associated with the nitridation level.[6] For instance, introduction of nitrogen in oxide NPs has shown advantages[7,8] in yielding remarkable band gap narrowing, noble-metal-like features, oxidation state changes, and electronic conductivity enhancement as well, enabling highly catalytic reactions. Consequently, modulation of materials properties by nitridation may be an effective strategy for the design of novel catalysts.

In this work, nitridation of a silent precursor, $Ta_{1.1}O_{1.05}$, was selected as the target to explore noble-metal-free and highly active catalysts for the reduction of 4-nitrophenol to 4-aminophenol. We first showed that the chemical composition and surface defect chemistry can be controlled simply through nitridation, which allows tuning of catalysts from silent to highly reactive. High-quality TaO_xN_y NPs with hollow structures were prepared using SiO_2 spheres as a hard template, $TaCl_5$ as the tantalum source, and NH_3 as the nitrogen source. Detailed experimental procedures are given in the Supporting Information (SI). Nitridation of the $Ta_{1.1}O_{1.05}$ precursor (Figure S1 in the SI) followed by removal of SiO_2 template afforded TaO_xN_y NPs, which showed a BET surface area of 22.8 m^2/g (Figure S4) and a hollow spherical structure (Figure 1a). The hollow structures were composed of tiny agglomerated nanocrystals. From the high-resolution transmission electron microscopy (HRTEM) image (Figure 1b), the spacing between adjacent lattice fringes was observed to be 0.309 nm, close to that of 0.306 nm calculated by X-ray diffraction (XRD). Further, XRD was used to confirm the crystallinity and phase purity of the TaO_xN_y nanocrystals (Figure 1c). The diffraction peaks matched well the standard data for TaON (JCPDS no. 70-1193). All of the diffraction peaks were significantly broadened, indicating the fine nature of the particles. The average crystallite size calculated from the broadening of the $(\bar{1}11)$ peak using the Scherrer formula was ~20 nm. The lattice parameters determined for the TaO_xN_y nanocrystals were a = 4.953 ± 0.002 Å, b = 5.016 ± 0.002 Å, c = 5.149 ± 0.002 Å, β =

Received: April 29, 2013
Published: July 24, 2013

dx.doi.org/10.1021/ja404239z | J. Am. Chem. Soc. 2013, 135, 11433−11436

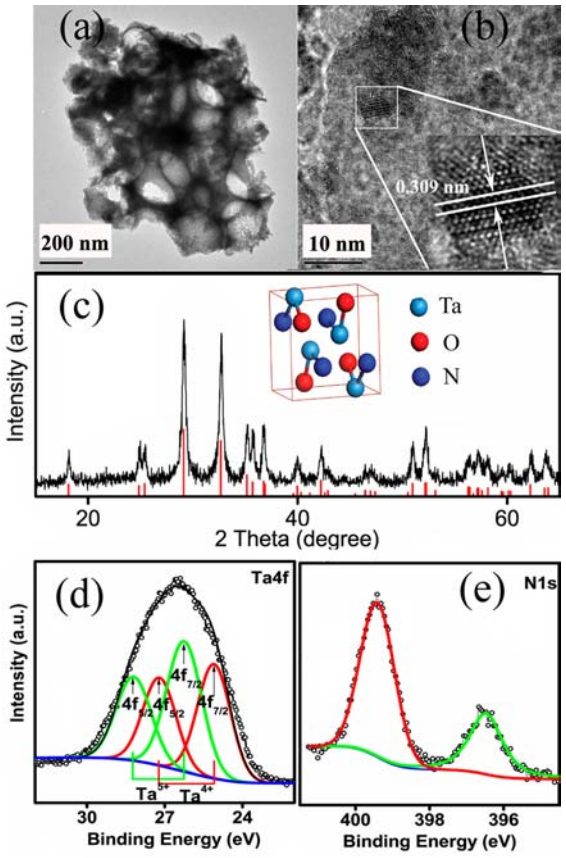

Figure 1. (a) TEM and (b) HRTEM images, (c) XRD pattern, and (d) Ta 4f and (e) N 1s XPS spectra of TaO_xN_y nanocrytals at $S_{N/O} = 0.14$. The inset in (c) shows the unit cell of TaON.

99.29 ± 0.02°, and $V = 126.24 \pm 0.05$ Å^3, all of which are smaller than those for the bulk (JCPDS no. 70-1193).

The chemical composition and oxidation states of the TaO_xN_y NPs were studied by X-ray photoelectron spectroscopy (XPS). Only one broad Ta 4f XPS signal was observed for the TaO_xN_y NPs (Figure 1d), in contrast to the well-resolved spin−orbit splitting of $4f_{7/2}$ and $4f_{5/2}$ for Ta_2O_5 and TaO_2. This broad XPS signal was fitted using a series of Lorentzian−Gaussian line shapes with the following triple restrictions: (i) the background was corrected according to the Shirley model; (ii) the peak full width at half-maximum was set in a range of 1.2−1.6 eV; and (iii) the ratio of the $4f_{7/2}$ and $4f_{5/2}$ peak areas was fixed at 1.33 with a fine-structure splitting distance of 1.9 eV. This showed that the broad Ta 4f core level contained two sets of doublets, one with binding energies (BEs) of 25.1 and 27.2 eV corresponding to $4f_{7/2}$ and $4f_{5/2}$ of Ta^{4+}, respectively, and the other with BEs of 26.3 and 28.2 eV corresponding to $4f_{7/2}$ and $4f_{5/2}$ of Ta^{5+}, respectively.[9] Therefore, the Ta ions in the TaO_xN_y nanocrystals were in a mixed-valence state of Ta^{4+} and Ta^{5+}, and their relative content was 47% Ta^{4+} and 53% Ta^{5+}.

Associated with the nonstoichiometry is the observation of N species in different chemical environments,[10] as confirmed by the observation of two N 1s signals at 396.3 and 399.4 eV (Figure 1e). Both signals were observed previously in other tantalum oxynitrides (Figure S5) and could be assigned to N^{3-} species in lattice sites[11] and interstitial sites.[12] For the former one, the difference in the N 1s and Ta^{5+} $4f_{7/2}$ BEs, $\Delta BE = BE_{N1s} - BE_{Ta4f_{7/2}}$ for TaO_xN_y nanocrystals was 370.2 eV, which is close to that previously reported for tantalum oxynitride,[13] further demonstrating the formation of TaO_xN_y nanocrystals. Further, on the basis of the characterization data analyses of N^{3-} species and Ta mixed-valence states, the 3 wt % N content determined by chemical analyses, and the single-phase nature with decreased lattice parameters, one may expect a nonstoichiometric composition of $x \approx 1.5$ and $y \approx 0.5$ for the TaO_xN_y nanocrystals. However, the surface N/O molar ratio ($S_{N/O}$) measured for the TaO_xN_y nanocrystals by XPS was only 0.14. The excess of oxygen species on the surface was due to the presence of abundant surface hydration layers, as indicated by the strong absorption around 3300 cm^{-1} in the IR spectrum (Figure S6).

The catalytic reduction of 4-nitrophenol to 4-aminophenol with excess $NaBH_4$ has often been used as a model reaction to evaluate the catalytic performance of various metallic NPs,[14] including Cu, Ni, Au, Ag, Pt, and Pd. The UV−vis absorption spectrum of an aqueous mixture of 4-nitrophenol and $NaBH_4$ had an absorption maximum at 400 nm, which is due to the formation of 4-nitrophenolate anions under alkaline conditions. In the absence of catalyst, the absorption peak remained unaltered with time, indicating that no reduction occurred (Figure S7). When a very small amount of TaO_xN_y NPs (0.3 mg) was added, the absorption at 400 nm decreased in intensity and a new peak appeared at 305 nm with a gradual intensity increase (Figure 2a), indicating the formation of 4-aminophenol (Figure S8).[15] The catalytic reduction efficiency of the TaO_xN_y nanocrystals was estimated to be 91.3% within a time interval of 45 min, which differs from silent $Ta_{1.1}O_{1.05}$ (Figure S9), Ta_2O_5 (Figures 2b and S10), and Ta_3N_5 (Figure S11).

The concentration of the main product, 4-aminophenol, in the reduction products was examined by mass spectrometry. The

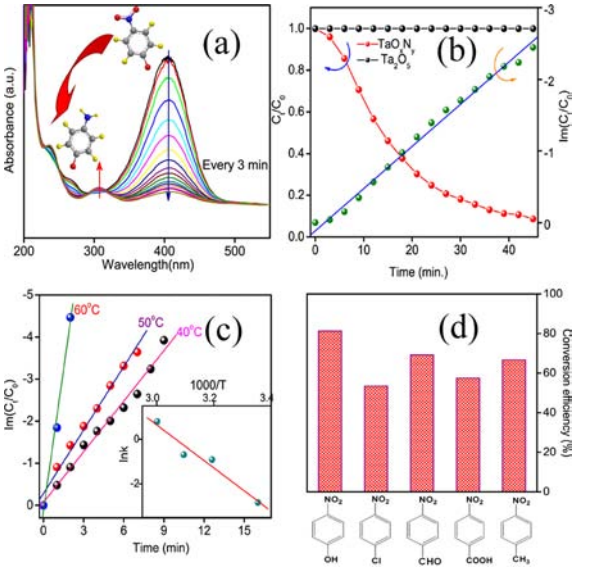

Figure 2. (a) UV−vis absorption spectra recorded during catalytic reduction of 4-nitrophenol over TaO_xN_y nanocrystals at 25 °C. (b) Residual fraction of 4-nitrophenol in solution as a function of reaction time (t) upon treatment with TaO_xN_y (red curve) or Ta_2O_5 (black curve) and the relation between $\ln(C_t/C_0)$ and t for TaO_xN_y treatment, wherein the ratio of the 4-nitrophenol concentration at time t to initial concentration (C_t/C_0) was obtained from the absorbance ratio A_t/A_0. The reduction course is reflected by these absorption curves. (c) Relationship between $\ln(C_t/C_0)$ and t for TaO_xN_y at different temperatures. The inset shows the Arrhenius plot for the reaction catalyzed by TaO_xN_y. (d) Conversion efficiencies in the initial 30 min for several substituted nitrobenzenes.

dx.doi.org/10.1021/ja404239z | J. Am. Chem. Soc. 2013, 135, 11433−11436

selectivity for 4-aminophenol was very high, since almost all initial 4-nitrophenol was transformed to 4-aminophenol (Figure S12). It is also noted here that the reduction started immediately after the addition of the catalyst, and no induction time was required. This might be advantageous for ease of use in real technological applications. Since excess $NaBH_4$ was employed, the reaction could be assumed to follow pseudo-first-order reaction kinetics with respect to 4-nitrophenol, which was confirmed by the linear plot of $\ln(C_t/C_0)$ versus t (Figure 2b). The apparent rate constant (k_{app}) determined from the slope was 5.9×10^{-2} min^{-1}. To compare our result with literature values, we calculated the ratio of apparent rate constant k_{app} to the total mass of the catalyst ($k = k_{app}/m$). The activity factor for the TaO_xN_y nanocrystals was $k = 196.7$ min^{-1} g^{-1}, which is much larger than those reported previously for several noble-metal NPs (Table S1 in the SI).

The catalytic reduction of 4-nitrophenol was studied at 40, 50, and 60 °C (Figure 2c) to determine k_{app} at these temperatures. From the linear fit of the Arrhenius plot ($\ln k_{app}$ vs $1000/T$), the apparent activation energy (E_a) was found to be 80.4 ± 12 kJ mol^{-1}, which is larger than those for most metallic NPs.[14c,16] Such a high E_a suggests a distinct reduction mechanism. More importantly, TaO_xN_y also exhibited excellent catalytic performance toward several aromatic nitro compounds. In the initial 30 min, the conversion efficiencies of TaO_xN_y for all of the nitro compounds were in the range from 53.5% to 81.3% (Figure 2d).

Numerous works have been dedicated to providing a mechanistic explanation of this reduction reaction, in which electron transfer from BH_4^- (−1.33 V vs. NHE) to 4-nitrophenol (−0.76 V vs. NHE) is mediated by surface metal atoms.[17] For the present TaO_xN_y nanocrystals, if Ta^{5+} ions at surfaces were the active centers, Ta_2O_5 NPs should be active for this reaction, which would contradict the experimental observations in Figure 2b. Moreover, two tantalate-based NPs, $NaTaO_3$ and $Sn_2Ta_2O_7$, were employed to test the reactivity of Ta^{5+} ions (Figure S13). No apparent activity was seen, which suggests that Ta^{5+} ions are likely irrelevant to the electron transfer process. To shed light on the underlying mechanism, we focused on the nitridation and its associated defect chemistry. From the viewpoint of solid-state physics, intrinsic defect centers such as oxygen vacancies are the most common defects in nanocrystalline semiconductors. To investigate the possibility that localized defects are responsible for the reduction process, electron spin resonance (ESR) measurements were performed on Ta_2O_5 and TaO_xN_y nanocrystals. Ta_2O_5 nanocrystals gave three separate resonances at g = 2.05, 2.02, and 1.97 (Figure 3a). The resonance at $g = 2.05$ is due to the surface-absorbed O_2^-,[18] while the ones at $g = 2.02$ and 1.97 are attributed to paramagnetic oxygen vacancies ($V_O^{\bullet}$), as documented for many oxide materials (e.g., TiO_2, CeO_2, ZnO, etc.).[19] Previous reports on TiO_2 have supposed that the reduction sites (i.e., Ti^{3+} and oxygen vacancies) are silent in the hydrogenation of 4-nitrophenol locating either in the bulk lattice or at surface sites.[5] This hypothesis was proved by the catalytic inertness of Ta_2O_5 nanocrystals and $Ta_{1.1}O_{1.05}$. After nitridation, all of the resonances for TaO_xN_y became weaker, and the resonance at $g = 2.05$ disappeared. In particular, the ESR signal at $g = 2.02$ was broadened and simultaneously slightly shifted to g = 2.03. This broadened signal may involve the contribution of oxygen vacancies overlapped with NO_x. These NO_x species are associated with interstitial nitrogen in TaO_xN_y, which may play critical roles in activating reduction processes.[10,20]

The O 1s signals in Figure 3b also showed significant changes upon nitridation (relative to Ta_2O_5 in Figure S14). The most

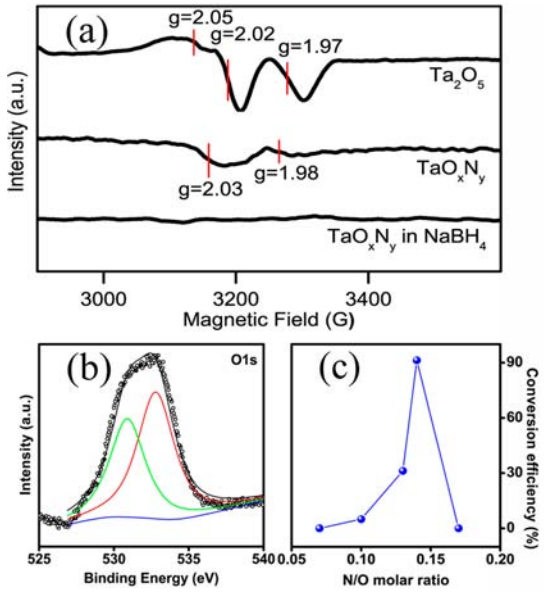

Figure 3. (a) ESR spectra of TaO_xN_y ($y/x = 0.14$), Ta_2O_5 nanocrystals, and TaO_xN_y in $NaBH_4$ solution. (b) O 1s XPS spectrum of TaO_xN_y. (c) Conversion efficiency of TaO_xN_y nanocrystals at different N/O molar ratios within a time frame of 45 min.

significant change is the appearance of an additional signal at a BE of 532.7 eV, which is somewhat higher than that for the main oxygen species. This new signal could originate from the formation of Ta−O−N bonds at oxynitride surfaces.[18] Nevertheless, NO_x species are not accessible to special reactive species to activate reduction by themselves, as indicated by the fact that the deep nitridation product Ta_3N_5 exhibited poor activity for reduction of 4-nitrophenol in the absence of paramagnetic oxygen vacancies at $g = 1.97$ (Figure S15).

On the basis of these results, it is expected that variations in the chemical composition of the TaO_xN_y nanocrystals may have great impacts on the catalytic performance. The 4-nitrophenol conversion efficiency gradually increased with N/O molar ratio, reaching a maximum at N/O = 0.14 (Figure 3c). The catalytic activity could be mainly related to NO_x species and oxygen vacancies. In a comparison of the O 1s signals for N/O = 0.14 (Figure 3b) with those for other molar ratios (Figure S16), the former sample showed the most intense XPS signal at 532.7 eV, which implies a high concentration of NO_x species. On the other hand, comparison of the ESR signals for N/O = 0.14 (Figure 3a) with those for other molar ratios (Figure S17) showed that TaO_xN_y nanocrystals at N/O = 0.14 exhibited a relatively strong ESR signal at $g = 2.03$. Therefore, TaO_xN_y nanocrystals have a highly defective surface structure, consistent with the nonstoichiometry. It should be mentioned that during nitridation, an abundant surface hydration layer was formed on the surfaces of TaO_xN_y nanocrystals as a result of the presence of the Ta^{4+}/Ta^{5+} mixed-valence state. The mixed-valence state facilitates electron transport,[8a] while surface hydration favors migration of proton species,[5] both of which could promote catalytic reactions. Since these defective structures always show high activity to absorb species that would act as donors of electrons or holes, it is reasonable that the synergetic effect of NO_x species and paramagnetic oxygen vacancies located at surfaces/interfaces dominates the adsorption and reduction of 4-nitrophenol.

It has been reported that BH_4^- adsorption is a fast and reversible process at the surfaces of metal nanocrystals and that

dx.doi.org/10.1021/ja404239z | J. Am. Chem. Soc. 2013, 135, 11433−11436

the reaction is dictated by coadsorption of 4-nitrophenolate ions, which may overcome the kinetic barrier for the reaction and initiate an interfacial electron transfer reaction.[21] To investigate the adsorption and surface rearrangement of BH_4^-, TaO_xN_y nanocrystals were dispersed in an aqueous $NaBH_4$ solution (0.04 M). In light of previous literature on N-doped TiO_2, it is known that nitrate species and imino functionality coexist in TiO_2. The imino species are regarded as an intermediate in the incomplete oxidation into nitrate species and can be transformed into nitrate species under an oxidative atmosphere.[22]

For TaO_xN_y nanocrystals, the nitrate species may convert to metastable iminoborohydride species by binding hydride ions from BH_4^- in a reductive environment. On the other hand, oxygen vacancies have been reported as the active sites for capture of oxygen of nitric oxide.[23] Therefore, a more plausible explanation is that oxygen vacancies act as the trap centers that capture the oxygen end of 4-nitrophenol molecules after addition of 4-nitrophenol. Mobile oxygen vacancies can diffuse close to metastable iminobrohydride species via a surface vacancy diffusion mechanism[24] and capture hydride ions on a neighboring site. Similar to the Langmuir−Hinshelwood mechanism, upon electron transfer and reaction of surface hydrogen species from iminobrohydride species, the 4-aminophenol species desorbs from the surface (Figure 4). Simultaneously, the BH_4^- ions help to release the trapped oxygen atoms from the lattice sites, resulting in the formation of borate ions. This was verified by our recycling experiment, in which the reducing capacity of TaO_xN_y nanocrystals was well-reserved after five cycles of redox reactions (Figure S18).

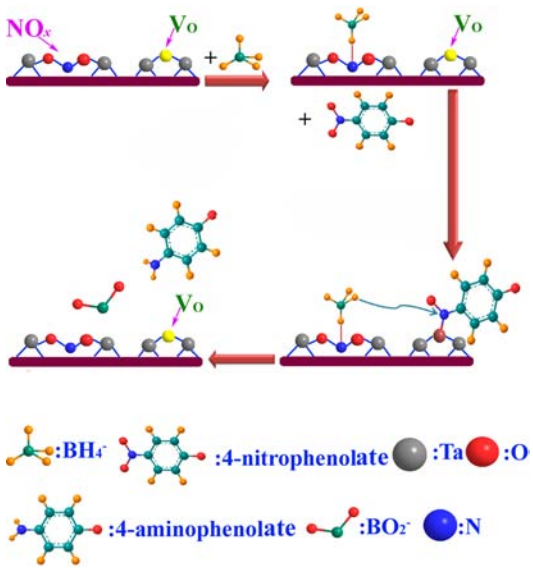

Figure 4. Illustration of possible reduction processes of 4-nitrophenol on the surfaces of TaO_xN_y nanocrystals.

In summary, a noble-metal-free and highly efficient catalyst was prepared by nitridation of a silent tantalum oxide to form a hollow nanostructure. Defective nitrogen species and oxygen vacancies were found to play the critical roles in the reduction of nitrobenzenes. The strategy reported here may open a realm of new possibilities for the development of novel defect-meditated catalytic systems and bring opportunities to many more electron transfer reactions that need to be catalyzed.

■ ASSOCIATED CONTENT

Supporting Information

Experimental details and additional data. This material is available free of charge via the Internet at http://pubs.acs.org.

■ AUTHOR INFORMATION

Corresponding Author

wang_xiao_jing@hotmail.com

Notes

The authors declare no competing financial interest.

■ ACKNOWLEDGMENTS

We thank the National Natural Science Foundation of China (21103081, 51102129, 21267014), the National Basic Research Program of China (2011CBA00501), and Fujian Provincial Key Lab of Nanomaterials (2006L2005) for support.

■ REFERENCES

(1) Maeda, Y.; Iizuka, Y.; Kohyama, M. *J. Am. Chem. Soc.* **2013**, *135*, 906.
(2) Najdovski, I.; Selvakannan, P. R.; Bhargava, S. K.; O'Mullane, A. P. *Nanoscale* **2012**, *4*, 6298.
(3) Zhang, X.; Su, Z. *Adv. Mater.* **2012**, *24*, 4574.
(4) He, S.; Li, C.; Chen, H.; Su, D.; Zhang, B.; Cao, X.; Wang, B.; Wei, M.; Evans, D. G.; Duan, X. *Chem. Mater.* **2013**, *25*, 1040.
(5) Su, J.; Zou, X.; Li, G.; Li, L.; Zhao, J.; Chen, J. *Chem. Commun.* **2012**, *48*, 9032.
(6) Xiong, Z. G.; Zhao, X. S. *J. Am. Chem. Soc.* **2012**, *134*, 5754.
(7) Gao, Q.; Wang, S.; Ma, Y.; Tang, Y.; Giordano, C.; Antonietti, M. *Angew. Chem., Int. Ed.* **2012**, *51*, 961.
(8) (a) Wang, D.; Jia, L.; Wu, X.; Lu, L.; Xu, A. *Nanoscale* **2012**, *4*, 576. (b) Wang, J.; Tafen, D. N.; Lewis, J. P.; Hong, Z.; Manivannan, A.; Zhi, M.; Li, M.; Wu, N. *J. Am. Chem. Soc.* **2009**, *131*, 12290.
(9) Hashimoto, S.; Tanaka, C.; Sakurada, T. *J. Surf. Anal.* **2006**, *13*, 14.
(10) Zou, F.; Jiang, Z.; Qin, X.; Zhao, Y.; Jiang, L.; Zhi, J.; Xiao, T.; Edwards, P. P. *Chem. Commun.* **2012**, *48*, 8514.
(11) Zhang, Z.; Wang, X.; Long, J.; Gu, Q.; Ding, Z.; Fu, X. *J. Catal.* **2010**, *276*, 201.
(12) Diwald, O.; Thompson, T. L.; Zubkov, T.; Goralski, E. G.; Walck, S. D.; Yates, J. T., Jr. *J. Phys. Chem. B* **2004**, *108*, 6004.
(13) Ho, C. T.; Low, K. B.; Klie, R. F.; Maeda, K.; Domen, K.; Meyer, R. J.; Snee, P. T. *J. Phys. Chem. C* **2011**, *115*, 647.
(14) (a) Patra, A. K.; Dutta, A.; Bhaumik, A. *Catal. Commun.* **2010**, *11*, 651. (b) Jiang, H.; Alita, T.; Ishida, T.; Haruta, M.; Xu, Q. *J. Am. Chem. Soc.* **2011**, *133*, 1304. (c) Bhandari, R.; Knecht, M. R. *Langmuir* **2012**, *28*, 8110.
(15) Wei, J.; Wang, H.; Deng, Y. H.; Sun, Z. K.; Shi, L.; Tu, B.; Luqman, M.; Zhao, D. Y. *J. Am. Chem. Soc.* **2011**, *133*, 20369.
(16) Zeng, J.; Zhang, Q.; Chen, J.; Xia, Y. N. *Nano Lett.* **2010**, *10*, 30.
(17) Zhang, Z.; Shao, C.; Sun, Y.; Mu, J.; Zhang, M.; Zhang, P.; Guo, Z. C.; Liang, P.; Wang, C.; Liu, Y. *J. Mater. Chem.* **2012**, *22*, 1387.
(18) Prokes, S. M.; Gole, J. L.; Chen, X. B.; Burda, C.; Carlos, W. E. *Adv. Funct. Mater.* **2005**, *15*, 161.
(19) Drouilly, C.; Krafft, J. M.; Averseng, F.; Casale, S.; Bazer-Bachi, D.; Chizallet, C.; Lecocq, V.; Vezin, H.; Lauron-Pernot, H.; Costentin, G. *J. Phys. Chem. C* **2012**, *116*, 21297.
(20) Barolo, G.; Livraghi, S.; Chiesa, M.; Paganini, M. C.; Giamello, E. *J. Phys. Chem. C* **2012**, *116*, 20887.
(21) Wunder, S.; Polzer, F.; Lu, Y.; Mei, Y.; Ballauff, M. *J. Phys. Chem. C* **2010**, *114*, 8814.
(22) Reyes-Garcia, E. A.; Sun, Y. P.; Reyes-Gil, K.; Raftery, D. *J. Phys. Chem. C* **2007**, *111*, 2738.
(23) Wu, Q. P.; van de Krol, R. *J. Am. Chem. Soc.* **2012**, *134*, 9369.
(24) Schaub, R.; Wahlström, E.; Rønnau, A.; Lægsgaard, E.; Stensgaard, I.; Besenbacher, F. *Science* **2003**, *299*, 377.